We demonstrate that loose coupling enables access of endogenous Ca^{2+} buffers acting as "brakes" on release probability. Second, our results shed light on the mechanism of presynaptic facilitation, a hallmark property of mossy fiber synapses (*13*, *15*, *26*). Loose coupling permits facilitation via saturation of endogenous Ca^{2+} buffers (*25*) (fig. S10). Last, our results have major implications for the mechanisms of long-term potentiation (LTP) at hippocampal mossy fiber synapses. Previous studies have shown that expression of mossy fiber LTP has a presynaptic locus but is not associated with a rise in the amplitude of global presynaptic Ca^{2+} transients (*39*). These results could be explained by a change in the coupling distance, a local change in the concentration of endogenous Ca^{2+} buffers, or a combination of both. This may allow faster onset of regulation of synaptic strength than a mechanism based on changes in the number of Ca^{2+} channels (*40*).

The large size of the presynaptic terminals and the proximal location of the synapse previously led to the idea that the mossy fiber synapse acts as an efficient "teacher" synapse in the network, driving the induction of heterosynaptic plasticity in synapses between CA3 cells (*41*, *42*). However, it is also widely accepted that mossy fiber synapses operate as conditional "detonators" (*28*). A single action potential in a presynaptic granule cell is not sufficient to trigger a spike in a postsynaptic CA3 pyramidal cell but needs to act in combination with presynaptic short-term plasticity. These properties are critical for network function, making the impact of the mossy fiber synapse dependent on burst activity in granule cells (*28*, *43*). Our results reveal that loose channel-sensor coupling and the presence of fast endogenous Ca^{2+} buffers are the key properties underlying the conditional detonator function of mossy fiber synapses. The switchlike nonlinearity conveyed by this specific design may assist in the separation of storage and retrieval modes in hippocampal memory circuits (*41*).

References and Notes

1. E. Neher, *Cell Calcium* **24**, 345–357 (1998).
2. C. J. Meinrenken, J. G. G. Borst, B. Sakmann, *J. Neurosci.* **22**, 1648–1667 (2002).
3. E. Eggermann, I. Bucurenciu, S. P. Goswami, P. Jonas, *Nat. Rev. Neurosci.* **13**, 7–21 (2012).
4. J. G. G. Borst, B. Sakmann, *Nature* **383**, 431–434 (1996).
5. M. J. Fedchyshyn, L. Y. Wang, *J. Neurosci.* **25**, 4131–4140 (2005).
6. I. Bucurenciu, A. Kulik, B. Schwaller, M. Frotscher, P. Jonas, *Neuron* **57**, 536–545 (2008).
7. J. M. Christie, D. N. Chiu, C. E. Jahr, *Nat. Neurosci.* **14**, 62–68 (2011).
8. A. Scimemi, J. S. Diamond, *J. Neurosci.* **32**, 18157–18176 (2012).
9. H. Schmidt *et al.*, *Curr. Biol.* **23**, 244–249 (2013).
10. T. H. Brown, D. Johnston, *J. Neurophysiol.* **50**, 487–507 (1983).
11. P. Jonas, G. Major, B. Sakmann, *J. Physiol.* **472**, 615–663 (1993).
12. J. R. P. Geiger, P. Jonas, *Neuron* **28**, 927–939 (2000).
13. R. A. Nicoll, D. Schmitz, *Nat. Rev. Neurosci.* **6**, 863–876 (2005).
14. J. Bischofberger, D. Engel, M. Frotscher, P. Jonas, *Pflugers Arch.* **453**, 361–372 (2006).
15. P. A. Salin, M. Scanziani, R. C. Malenka, R. A. Nicoll, *Proc. Natl. Acad. Sci. U.S.A.* **93**, 13304–13309 (1996).
16. S. Nadkarni, T. M. Bartol, C. F. Stevens, T. J. Sejnowski, H. Levine, *Proc. Natl. Acad. Sci. U.S.A.* **109**, 14657–14662 (2012).
17. R. Schneggenburger, A. C. Meyer, E. Neher, *Neuron* **23**, 399–409 (1999).
18. H. von Gersdorff, J. G. G. Borst, *Nat. Rev. Neurosci.* **3**, 53–64 (2002).
19. E. M. Adler, G. J. Augustine, S. N. Duffy, M. P. Charlton, *J. Neurosci.* **11**, 1496–1507 (1991).
20. A. Rollenhagen *et al.*, *J. Neurosci.* **27**, 10434–10444 (2007).
21. B. Katz, R. Miledi, *J. Physiol.* **195**, 481–492 (1968).
22. M. Blatow, A. Caputi, N. Burnashev, H. Monyer, A. Rozov, *Neuron* **38**, 79–88 (2003).
23. F. Felmy, E. Neher, R. Schneggenburger, *Neuron* **37**, 801–811 (2003).
24. R. S. Zucker, W. G. Regehr, *Annu. Rev. Physiol.* **64**, 355–405 (2002).
25. A. Rozov, N. Burnashev, B. Sakmann, E. Neher, *J. Physiol.* **531**, 807–826 (2001).
26. K. Toth, G. Suares, J. J. Lawrence, E. Philips-Tansey, C. J. McBain, *J. Neurosci.* **20**, 8279–8289 (2000).
27. J. J. Lawrence, Z. M. Grinspan, C. J. McBain, *J. Physiol.* **554**, 175–193 (2004).
28. D. A. Henze, L. Wittner, G. Buzsáki, *Nat. Neurosci.* **5**, 790–795 (2002).
29. M. S. Thanawala, W. G. Regehr, *J. Neurosci.* **33**, 4625–4633 (2013).
30. M. Pusch, E. Neher, *Pflugers Arch.* **411**, 204–211 (1988).
31. E. Eggermann, P. Jonas, *Nat. Neurosci.* **15**, 20–22 (2012).
32. V. Matveev, R. S. Zucker, A. Sherman, *Biophys. J.* **86**, 2691–2709 (2004).
33. M. D. Brandt *et al.*, *Mol. Cell. Neurosci.* **24**, 603–613 (2003).
34. A. Müller *et al.*, *J. Neurosci.* **25**, 558–565 (2005).
35. B. Schwaller, *Cold Spring Harb. Perspect. Biol.* **2**, a004051 (2010).
36. G. C. Faas, S. Raghavachari, J. E. Lisman, I. Mody, *Nat. Neurosci.* **14**, 301–304 (2011).
37. M. E. Chicurel, K. M. Harris, *J. Comp. Neurol.* **325**, 169–182 (1992).
38. S. Hallermann, C. Pawlu, P. Jonas, M. Heckmann, *Proc. Natl. Acad. Sci. U.S.A.* **100**, 8975–8980 (2003).
39. H. Kamiya, K. Umeda, S. Ozawa, T. Manabe, *J. Neurosci.* **22**, 10524–10528 (2002).
40. J. Sheng *et al.*, *Nat. Neurosci.* **15**, 998–1006 (2012).
41. A. Treves, E. T. Rolls, *Hippocampus* **2**, 189–199 (1992).
42. K. Kobayashi, M. M. Poo, *Neuron* **41**, 445–454 (2004).
43. J. E. Lisman, *Trends Neurosci.* **20**, 38–43 (1997).

Acknowledgments: We thank E. Neher and R. Shigemoto for critically reading the manuscript, F. Marr and M. Duggan for technical assistance, A. Solymosi for manuscript editing, and the scientific service units of IST Austria for efficient help. Supported by the Fond zur Förderung der Wissenschaftlichen Forschung (P 24909-B24) and the European Union (European Research Council Advanced Grant 268548 to P.J.).

Supplementary Materials

www.sciencemag.org/content/343/6171/665/suppl/DC1
Materials and Methods
Figs. S1 to S10
Table S1
References (*44*–*59*)

16 August 2013; accepted 11 December 2013
10.1126/science.1244811

Local Impermeant Anions Establish the Neuronal Chloride Concentration

J. Glykys,[1]* V. Dzhala,[1]* K. Egawa,[1]* T Balena,[1] Y. Saponjian,[1] K. V. Kuchibhotla,[2] B. J. Bacskai,[1] K. T. Kahle,[3] T. Zeuthen,[4] K. J. Staley[1]†

Neuronal intracellular chloride concentration $[Cl^-]_i$ is an important determinant of γ-aminobutyric acid type A ($GABA_A$) receptor ($GABA_AR$)–mediated inhibition and cytoplasmic volume regulation. Equilibrative cation-chloride cotransporters (CCCs) move Cl^- across the membrane, but accumulating evidence suggests factors other than the bulk concentrations of transported ions determine $[Cl^-]_i$. Measurement of $[Cl^-]_i$ in murine brain slice preparations expressing the transgenic fluorophore Clomeleon demonstrated that cytoplasmic impermeant anions ($[A]_i$) and polyanionic extracellular matrix glycoproteins ($[A]_o$) constrain the local $[Cl^-]$. CCC inhibition had modest effects on $[Cl^-]_i$ and neuronal volume, but substantial changes were produced by alterations of the balance between $[A]_i$ and $[A]_o$. Therefore, CCCs are important elements of Cl^- homeostasis, but local impermeant anions determine the homeostatic set point for $[Cl^-]$, and hence, neuronal volume and the polarity of local $GABA_AR$ signaling.

The γ-aminobutyric acid type A ($GABA_A$) receptor ($GABA_AR$) can subserve either inhibition or excitation, because the net flux of the permeating anions HCO_3^- and Cl^- can be reversed by modest changes in the transmembrane concentration gradient of Cl^- (*1*, *2*). NKCC1 and KCC2 are the primary cation-chloride cotransporters (CCCs) in neurons (*3*). Their unique stoichiometries result in distinct $[Cl^-]_i$ equilibria: ~3 mM for KCC2 (*4*, *5*) and ~60 mM for NKCC1 (*3*). The species of cotransporter expressed in the neuron is thought to determine $[Cl^-]_i$, but there is evidence that transporter expression is not the sole determinant of $[Cl^-]_i$ and, hence, the reversal potential for GABA (E_{GABA}). First, CCCs transport water along with cations and Cl^- as nearly isotonic saline (*6*, *7*). Neurons express no known aquaporin water channels (*8*), so the CCCs have limited capacity to alter $[Cl^-]_i$ independently of neuronal volume. Second, the transporter expressed may not correlate with the measured $[Cl^-]_i$ (*9*). Third, electrophysiological and fluorometric studies demonstrate a wide distribution

[1]Department of Neurology, Massachusetts General Hospital, Harvard Medical School, Boston, MA 02115, USA. [2]Skirball Institute for Biomolecular Medicine, New York University School of Medicine, New York, NY 10016, USA. [3]Department of Neurosurgery, Massachusetts General Hospital, Harvard Medical School, Boston, MA 02115, USA. [4]Department of Cellular and Molecular Medicine, University of Copenhagen, 2200 Copenhagen, Denmark.

*These authors contributed equally to this work.
†Corresponding author. E-mail: staley.kevin@mgh.harvard.edu

of $[Cl^-]_i$ that rarely matches the equilibrium for either NKCC1 or KCC2 (*10*–*15*). Finally, subcellular differences in E_{GABA} indicate that $[Cl^-]_i$ is likely to vary within the cytoplasm of individual neurons (*16*, *17*), a condition that cannot be efficiently maintained solely by transporters because of the high rate of dissipation of local $[Cl^-]_i$ by cytoplasmic diffusion (*18*).

A solution is suggested by the fact that Cl^- is only a minor component of the intracellular anionic milieu. The neuronal membrane is impermeable to most cytoplasmic anions, including phosphate groups associated with deoxy- and ribonucleotides, and the majority of intracellular proteins whose amino and carboxyl moieties are negatively charged at physiological pH (*19*). For any value of cytoplasmic volume and osmolarity, the sum of cytoplasmic impermeant anions ($[A]_i$) and $[Cl^-]_i$ must be constant, as $[HCO_3^-]$ is fixed by pH requirements. Thus, $[Cl^-]_i$ should be constrained by $[A]_i$. However, cotransport of Cl^- and cations across a membrane that is impermeant to $[A]_i$ creates an unstable Gibbs-Donnan condition with higher intracellular than extracellular osmotic pressure (*20*). The exclusion of Na^+ from the cytoplasm by Na^+- and K^+-dependent adenosine triphosphatase (Na^+,K^+-ATPase) is thought to create a balancing Gibb-Donnan condition (*7*, *20*), but this mechanism ignores intracellular K^+ and is not supported by pharmacological inhibition of neuronal Na^+,K^+-ATPase (*21*). The sulfates on the proteoglycans of the extracellular matrix (*22*) make up a more plausible impermeant extracellular ion. Manipulation of extracellular proteoglycans alters cell volume, membrane potential, and neuronal network excitability, consistent with Donnan effects (*23*). We investigated whether $[Cl^-]_i$ is set by the local concentrations of impermeant anions on either side of the neuronal membrane.

Direct $[Cl^-]_i$ measurements were performed by using two-photon excitation microscopy imaging in acute and organotypic brain slices of mice expressing Clomeleon [ratiometric fluorophore sensitive to changes in $[Cl^-]_i$ (*18*)]. In neonatal neurons from CA1 hippocampal slices from postnatal day 8 to 9 (P8 to P9), where NKCC1 is the primary transporter expressed (*24*), there was a broad distribution of somatic $[Cl^-]_i$ of 14.7 ± 6.5 mM (median ± SD; $n = 237$ neurons; six slices) (Fig. 1, A and B). In adult CA1 hippocampal slices (P32 to P44), where KCC2 is the primary transporter (*3*), the somatic $[Cl^-]_i$ was also widely distributed 13.7 ± 8.9 mM ($n = 227$ neurons; eight slices) (Fig. 1C). Similar results were found in acute brain slices from neocortex layers IV/V and CA1 organotypic hippocampal slices (figs. S1,

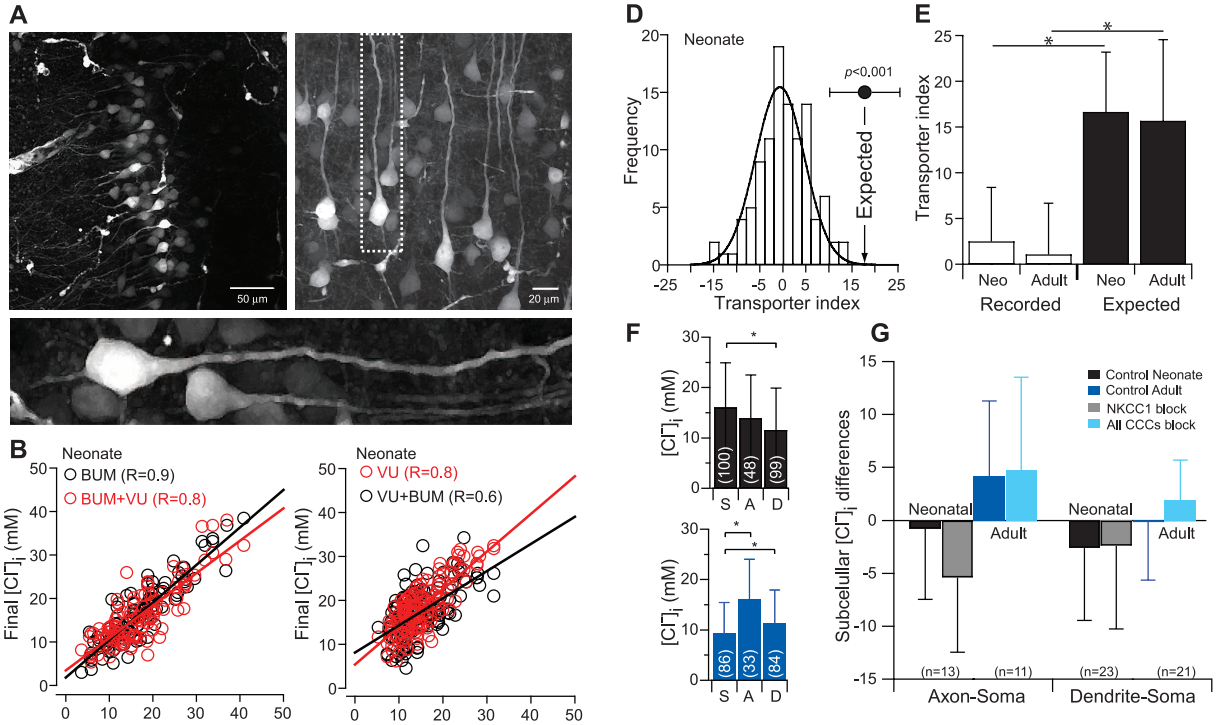

Fig. 1. $[Cl^-]_i$ is not solely determined by transport activity. (**A**) Two-photon microscopy image of Clomeleon yellow fluorescent protein (YFP) from acute hippocampal slice CA1 (left) and neocortex layer IV/V (right). (Bottom) Detailed image of neuron outlined on right above. (**B**) P8 to P9 hippocampal slice. (Left) Initial versus new steady-state $[Cl^-]_i$ after 30-min NKCC1 block followed by an additional 30-min block of KCC2. Lines, linear fit. (Right) Similar to left but KCC2 block was first, followed by KCC2 and NKCC1 blocks. (**C**) As (B) but in P32 to P44 CA1 neurons. (**D**) Transporter index histogram of all neonatal hippocampal neurons (calculated as in methods and fig. S5), 2.5 ± 5.9 ($n = 237$; median ± SD). Black circle indicates expected value for canonical cooperation of KCC2 and NKCC1. (**E**) Transporter index of all recorded neonatal CA1 neurons (2.5 ± 5.9) and adult CA1 neurons (1.07 ± 5.6; $n = 227$) and expected values (neonatal: 16.7 ± 6.5; $n = 237$; adult: 15.7 ± 8.9; $n = 227$). *$P < 0.001$, Mann-Whitney rank-sum test. (**F**) (Top) $[Cl^-]_i$ from P6 to P8 layer IV/V neocortical pyramidal cells [soma (S): 16.0 ± 8.9 mM; axon (A): 13.9 ± 8.6 mM; dendrite (D): 11.5 ± 8.3 mM; difference among all three groups, $P < 0.001$, Friedman test; *$P < 0.05$ multiple-comparison Dunn's method]. (Bottom) $[Cl^-]_i$ from P28 to P30 layer IV/V neocortical pyramidal cells [soma (S): 9.3 ± 6.1 mM; axon (A): 16.1 ± 7.9 mM; dendrite (D): 11.4 ± 6.5 mM; *$P < 0.001$]. (**G**) Subcellular gradient differences between axon-soma and dendrite-soma. Blockade of NKCC1 in neonates (10 µM bumetanide) and NKCC1 and KCC2 in adults (100 µM bumetanide) did not alter the subcellular $[Cl^-]_i$ gradients (paired neuron-process; $P > 0.05$; paired *t* test, error bars, SD).

A and C, and S2, A and B; and tables S1 and S2). Thus, most neurons have $[Cl^-]_i$ not congruent with the equilibrium conditions of either KCC2 or NKCC1.

If $[Cl^-]_i$ was primarily maintained by CCCs, the change in $[Cl^-]_i$ after transport block should be the opposite of the canonical direction of the primary expressed transporter: KCC2 block should increase $[Cl^-]_i$; NKCC1 block should decrease $[Cl^-]_i$. In neonatal CA1 slices (P8 to P9), blocking NKCC1 with bumetanide 10 μM did not alter $[Cl^-]_i$ (15.8 ± 7.6 to 16 ± 7.3 mM, $n = 105$ paired cells) (Fig. 1B and fig. S3A). Addition of 10 μmol of the specific KCC2 antagonist VU0240551 (*25*) induced a minimal decrease in $[Cl^-]_i$ to 15 ± 6.9 mM (Fig. 1B and fig. S3A), and $[Cl^-]_i$ did not become passively distributed across the membrane such that the reverse potential for Cl^- (E_{Cl}) ≈ resting membrane potential. After CCC block, $[Cl^-]_i$ increased in neurons with a low initial $[Cl^-]_i$ and decreased in neurons with a high initial $[Cl^-]_i$ (fig. S3A), regardless of the order of antagonist application (Fig. 1B and fig. S3B) in adult CA1 slices (P32 to P44) (Fig. 1C and fig. S3, C and D), in CA1 organotypic hippocampal slices after 6 to 11 days in vitro (DIV6 to DIV11) (fig. S2, A to C and E to G), and in acute layer IV/V neocortical pyramidal neurons (P8 to P9 and P27 to P31) (fig. S1 and tables S1 and S2). If no drug was added, $[Cl^-]_i$ was stable (fig. S4, C to E). In summary, the initial $[Cl^-]_i$ was a better predictor of the change in $[Cl^-]_i$ than was the species of blocked transporter. To quantify this, we summed the absolute values of the change in $[Cl^-]_i$ during sequential block of KCC2 and NKCC1. If NKCC1 and KCC2 are working against each other in the same neuron to create a broad distribution of $[Cl^-]_i$, this sum value should be large (fig. S5). However, this sum was nearly 0 in all neuronal populations studied (Fig. 1, D and E, and fig. S2, D and H). Therefore, the broad distribution of $[Cl^-]_i$ cannot be explained by the net effects of oppositely directed NKCC1 and KCC2 cotransport.

$[Cl^-]_i$ varies not only between neurons but also between subcellular regions (*16*), which is difficult to reconcile with the high intracellular mobility of $[Cl^-]_i$ (*18*). We measured millimolar differences in $[Cl^-]_i$ at the soma versus the proximal 40 μm of the axon and the proximal 200 μm of the apical dendrites of neonatal and adult neocortical neurons (sparse neocortical expression of Clomeleon permitted identification of individual processes and soma) (Fig. 1F). Subcellular differences in $[Cl^-]_i$ were not maintained by local CCCs because, after CCC block, $[Cl^-]_i$ gradients were unchanged ($P > 0.05$, paired t test) (Fig. 1G).

These data are not consistent with the hypothesis that $[Cl^-]_i$ is determined by the species of expressed cotransporter. Rather, the data suggest that KCC2 and NKCC1 both serve as conduits for transmembrane Cl^- flux whose direction is determined by other factor(s). We therefore tested the hypothesis that $[A]_i$ and the polyanionic extracellular matrix glycoproteins $[A]_o$ determine the local $[Cl^-]$ and, thus, E_{Cl} and the effect of $GABA_A$ receptor activation.

Prediction 1. If the sum of $[A]_i + [Cl^-]_i$ is constant, then the broad distribution of $[Cl^-]_i$, together with the large intercellular variance in the primary constituents of $[A]_i$ [cytoplasmic protein and nucleic acid concentrations (*26*)], can be used to test for the predicted reciprocal relation between $[A]_i$ and $[Cl^-]_i$. $[A]_i$ and $[Cl^-]_i$ were imaged in Clomeleon organotypic hippocampal slice cultures to facilitate the prolonged dye incubation required to estimate $[A]_i$. CA1 pyramidal neurons demonstrated a wide range of somatic $[Cl^-]_i$ of 14.8 ± 6.3 mM at DIV10 to DIV12 ($n = 305$ neurons; four slices) (Fig. 2, A to C). After Cl^- imaging, slices were incubated for 2 hours in SYTO64 10 μM, which binds to the cytoplasmic-nuclear nucleic

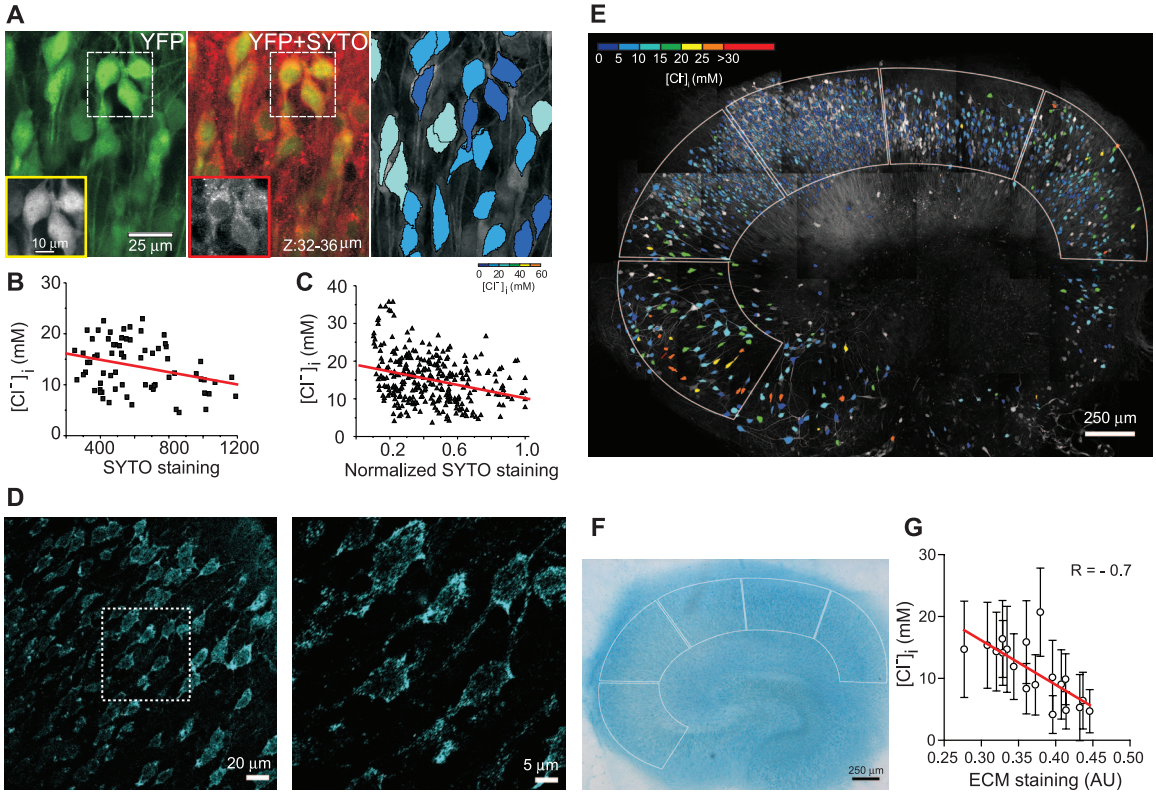

Fig. 2. Correlation of $[A]_i$ and $[A]_o$ with neuronal $[Cl^-]_i$. (**A**) (Left) Two-photon microscopy *z*-stack image of YFP (green) from CA1 pyramidal layer in an organotypic hippocampal slice from a Clomeleon-expressing mouse. (Middle) SYTO64 staining (red) of cytoplasmic and nuclear nucleic acids overlaid on the YFP image. (Boxes) YFP and SYTO64 fluorescence in individual neurons. (Right) Pseudo-colored neurons on the basis of the YFP/CFP (cyan fluorescent protein) ratio. (**B**) $[Cl^-]_i$ as a function of SYTO64 staining. $R = -0.29$, $P = 0.01$; $n = 70$ neurons; one slice. (**C**) $[Cl^-]_i$ as a function of normalized SYTO64 staining. $R = -0.3$, $P < 0.001$; $n = 305$ neurons; four slices. Line, linear fit. (**D** to **F**) Correlation between sulfated extracellular matrix and $[Cl^-]_i$. (D) Confocal images of Alcian blue staining in CA1 pyramidal layer of an organotypic hippocampal slice. Outlined area magnified on right. (E) $[Cl^-]_i$ distribution before Alcian blue staining. Outlines: Region of interest used to calculate average $[Cl^-]_i$ and Alcian blue staining intensity. (F) Alcian blue staining of slice in (E), transmitted light. (**G**) Correlation between $[Cl^-]_i$ and extracellular matrix (Alcian blue staining) obtained in each region of interest, four slices. Error bars, SD; AU, arbitrary units. Line, linear fit ($P < 0.001$).

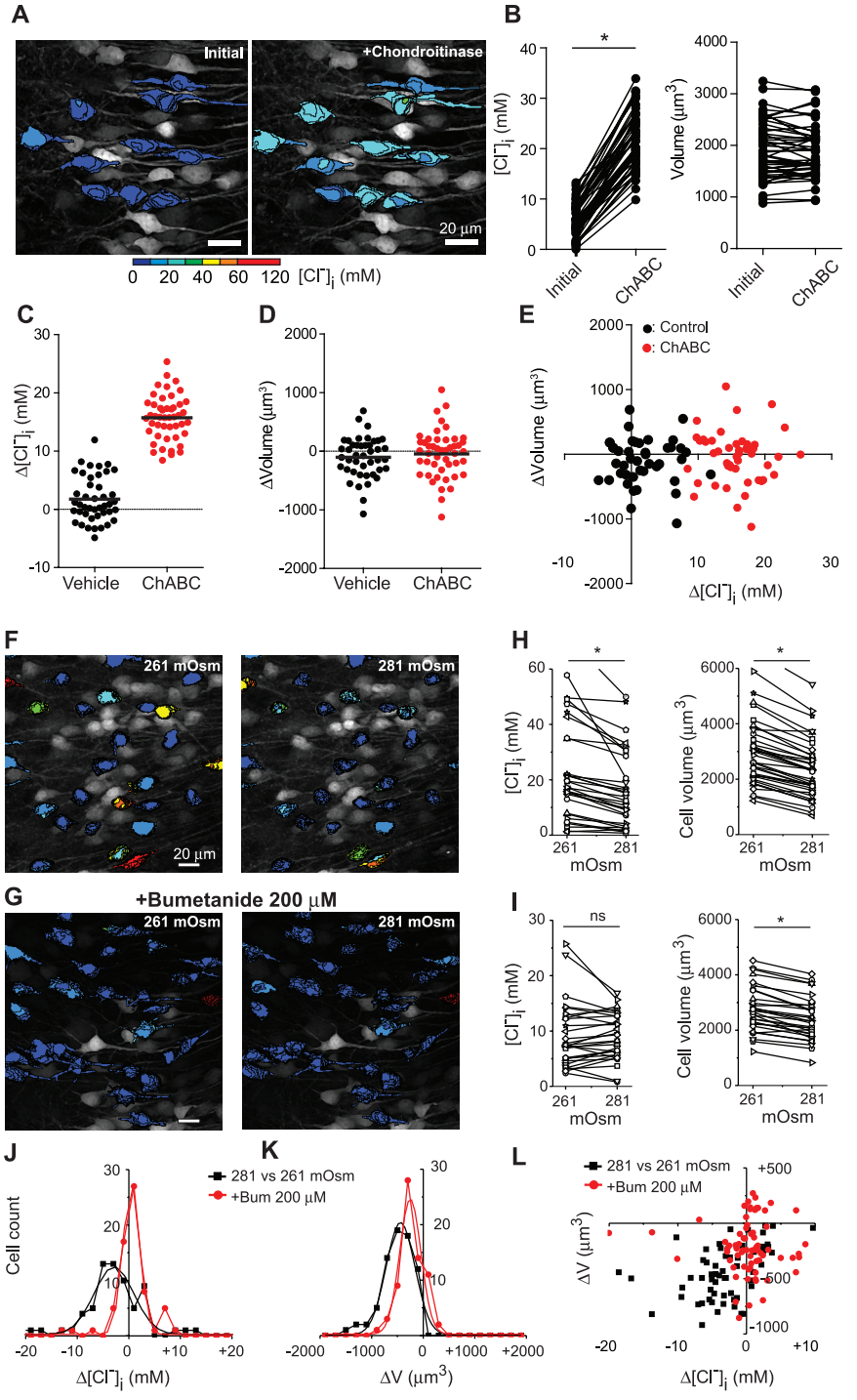

Fig. 3. $[Cl^-]_i$ is changed by disruption of the extracellular matrix and by increased extracellular osmolarity. (**A**) Pseudo-colored, two-photon microscopy z-stack image before and after incubation with chondroitinase ABC (ChABC) in an organotypic hippocampal slice. (**B**) Significant effect of ChABC on $[Cl^-]_i$, but not volume. (**C**) $[Cl^-]_i$ change by incubation with vehicle versus ChABC solution (vehicle: +0.8 ± 3.9 mM, $n = 43$; four slices; ChABC: +15.8 ± 3.8 mM, $n = 47$; four slices; $P < 0.0001$, unpaired t test). (**D**) As in (C) but plotting somatic volume (vehicle; −52 ± 174 μm³, ChABC; −23 ± 203 μm³, $P = 0.46$ unpaired t test. Change in vehicle: 1699 ± 480 to 1647 ± 464 μm³, $P = 0.08$. Change in ChABC: 1905 ± 564 to 1882 ± 516 μm³, $P = 0.51$, Wilcoxon signed rank test, same cells as (C). (**E**) Volume versus $[Cl^-]_i$ changes for each neuron in (C) and (D). *$P < 0.0001$. (**F** and **G**) Organotypic hippocampal slices expressing Clomeleon (two-photon microscopy) after increasing osmolarity with 20 mM mannitol (8% increase) and in bumetanide (G). (**H** and **I**) $[Cl^-]_i$ and neuronal volume changes in mannitol (H) and mannitol plus bumetanide (I). (**J** and **K**) $[Cl^-]_i$ and neuronal somatic volume changes induced by increased extracellular osmolarity. (**L**) Neuronal volume changes as a function of $[Cl^-]_i$ changes.

acids whose phosphate groups are a major component of $[A]_i$. SYTO64 staining intensity was negatively correlated with $[Cl^-]_i$ [correlation coefficient (R) = −0.3; $P < 0.001$] (Fig. 2, B and C). Because nucleic acids make up approximately one-third of intracellular fixed anions (*27*), the strength of the correlation between SYTO64 staining and $[Cl^-]_i$ is what would be predicted if $[A]_i$ sets $[Cl^-]_i$.

Prediction 2. If the sum of $[A]_i$ and $[Cl^-]_i$ is constant, then increasing $[A]_i$ should decrease $[Cl^-]_i$. $[A]_i$ was increased by iso-osmotic perfusion of 20 mM gluconate, pyruvate, and D-lactate, which are weak organic acids that are transported across the cytoplasmic membrane (*28*). Each perfusion reduced $[Cl^-]_i$ by 5 to 10%, consistent with a corresponding increase in $[A]_i$ due to a Nernstian distribution of the deprotonated, anionic bases at a resting membrane potential near −70 mV (fig. S6). This was unlikely a pH effect on Clomeleon fluorescence, because the pH_i effects (*29*) would alter Clomeleon fluorescence in the opposite direction from those observed (*18*). Thus, increases in $[A]_i$ are accompanied by reductions in $[Cl^-]_i$, so that the sum of $[A]_i + [Cl^-]_i$ is constant.

Prediction 3. If $[A]_o$ sets the local extracellular chloride concentration $[Cl^-]_o$, then cation-chloride cotransport should come to equilibrium at a $[Cl^-]_i$ that reflects the local $[Cl^-]_o$. Thus, $[A]_o$ should vary inversely with $[Cl^-]_i$. The polysulfated proteoglycans of the extracellular matrix create extracellular negative charge densities of 50 to 350 mEq/liter and, thus, could compose $[A]_o$ (*30*). We first verified that extracellular Na^+ does not exert a significant Donnan effect (*21*) (fig. S7). Next, $[Cl^-]_i$ was measured in organotypic Clomeleon hippocampal slices (DIV12 to DIV14). Then, slices were fixed and incubated with Alcian blue at pH 0.5 to specifically stain sulfated glycosaminoglycans (*31*). $[A]_o$ as assayed by Alcian blue staining was negatively correlated with $[Cl^-]_i$ ($R = -0.7$, $P < 0.001$) (Fig. 2, D to G, and fig. S8). These data support the possibility that polysulfated proteoglycans of the extracellular matrix make up $[A]_o$ and that, together with $[A]_i$, these macromolecular anions constrain the local $[Cl^-]$ to set the local E_{Cl}.

Prediction 4. Decreasing $[A]_o$ will increase $[Cl^-]_i$. If the sulfated carbohydrate moieties of the proteoglycans in the extracellular matrix subserve this function, then their lysis would release SO_4^- and reduce $[A]_o$. This would increase local $[Cl^-]_o$ and shift the equilibrium condition for transmembrane cation-chloride transport toward higher $[Cl^-]_i$. Accordingly, when organotypic hippocampal slices (DIV12 to DIV14) were incubated in chondroitinase ABC (ChABC) for 1 hour, neuronal $[Cl^-]_i$ increased from 5.9 ± 3.4 to 20.2 ± 5.7 mM ($n = 47$ neurons; four slices, $P < 0.0001$, Wilcoxon signed rank test) (Fig. 3, A to E). The $[Cl^-]_i$ change was significantly higher ($P < 0.0001$) than that by incubation with vehicle solution (from 9.2 ± 2.7 to 10.9 ± 4.3 mM, $n = 43$; four slices, $P = 0.02$). Somatic volume was unchanged at ~80 min (Fig. 3, B, D, and E), which likely

reflects successful compensatory volume regulation. Cell viability was not altered by incubation in ChABC (fig. S9).

Prediction 5. In a system in which $[A]_i$, $[A]_o$, and $[Cl^-]_i$ are in ionic and osmotic equilibrium, acutely altering the osmotic balance should alter $[Cl^-]_i$. Water is transported with cations and Cl^- by CCCs (*6*, *7*), and neurons lack known aquaporins (*8*). Thus, water movement contributes to the free energy of cotransport (*6*). An increase in extracellular osmolarity would favor CCC movement of water and Cl^- out of the neuron, increasing the fractional cytoplasmic concentration of $[A]_i$ and decreasing $[Cl^-]_i$. This is opposite to what would be predicted by free transmembrane water permeability: Loss of intracellular water would increase $[Cl^-]_i$ (*7*). Two-photon multiplanar micrographs of individual pyramidal cells from organotypic hippocampal slices (DIV8 to DIV12) expressing Clomeleon were reconstructed in three dimensions to measure volume and $[Cl^-]_i$ (Fig. 3, F to I). In control conditions, the somatic volume and $[Cl^-]_i$ were stable as a function of time (fig. S4). Increasing extracellular osmolarity by 8% [from 261 (the osmolarity of culture medium) to 281 mOsm] via the addition of 20 mM mannitol resulted in a rapid 21% decrease in somatic volume from 2333 ± 1192 to 1842 ± 967 μm^3 (mean ± SD, n = 73 neurons; four slices; $P <$ 0.001, paired t test) and a 9% decrease in somatic $[Cl^-]_i$ from 16.6 ± 14.6 to 15.1 ± 11.1 mM ($P <$ 0.001, Wilcoxon signed rank test) (Fig. 3, H, J, and L). Using the same protocol but blocking NKCC1 and KCC2 (with bumetanide 200 μM) resulted in a 9% decrease in somatic volume from 2365 ± 1005 to 2147 ± 953 μm^3 (n = 68 neurons; three slices; $P < 0.0001$, paired t test) (Fig. 3, I and K) and no change in somatic $[Cl^-]_i$ from 7.1 ± 10 to 8.3 ± 7.9 mM (P = 0.074, Wilcoxon signed rank test) (Fig. 3, I to L). The unlinking of volume and $[Cl^-]_i$ changes when CCCs were blocked is likely to represent volume regulation by other systems (*7*).

Finally, a consequence of the cotransport of water and salt by NKCC1 and KCC2 is that near-isotonic saline moves across the membrane, so that both neuronal volume and $[Cl^-]_i$ should change in parallel during cotransport. Several conditions—including hypoxic ischemic injury, trauma, and prolonged seizures—have in common the development of cytotoxic edema and increased neuronal $[Cl^-]_i$ (*15*, *32*, *33*). To test whether seizure-induced increases in neuronal volume are associated with acute increases in $[Cl^-]_i$, we performed extracellular field recording and two-photon microscopy to measure cytoplasmic volume and $[Cl^-]_i$ in organotypic hippocampal slice cultures (DIV10 to DIV12) that spontaneously develop ictal-like epileptiform discharges (*34*). Prolonged seizure activity increased both neuronal volume and $[Cl^-]_i$ (Fig. 4). Somatic volume increased by 10% from 2530 ± 1658 to 2775 ± 1741 μm^3 (mean ± SD; n = 42 neurons; four slices; P = 0.006, paired t test) and $[Cl^-]_i$ increased from 25.4 ± 7.4 to 40.8 ± 13.8 mM ($P <$ 0.001, Wilcoxon signed rank test). The increase in $[Cl^-]_i$ during seizures is mediated by NKCC1 as it can be reduced by bumetanide (*15*).

These data indicate that the local $[A]_i$ and $[A]_o$ determine $[Cl^-]_i$, $[Cl^-]_o$, and, thus, E_{GABA}, and CCCs serve to maintain $[Cl^-]_i$ at this set point. Therefore, (i) the widely observed intercellular and intracellular variances in $[Cl^-]_i$ and E_{GABA} are best explained by local variation in $[A]_i$ and $[A]_o$. The species of CCC and other cellular features are likely to correlate with $[A]_i$ and $[Cl^-]_i$ [e.g., (*14*, *24*)]. (ii) The developmental reduction in $[Cl^-]_i$ would follow from the increase in neuronal $[A]_i$ during development (*35*) and experience (*36*), paralleled by increases in the proteoglycans of the extracellular matrix (*37*). (iii) The subcellular variance in $[Cl^-]_i$ arises from corresponding differences in the concentrations of relatively immobile cytoplasmic macromolecular anions (*38*). The variance in $[A]_i$ creates intracytoplasmic Gibbs-Donnan effects (*39*), such that local $[Cl^-]_i$ is at equilibrium at different local $[A]_i$. Thus, CCCs are not required to compensate for intracytoplasmic Cl^- diffusion. (iv) The influence

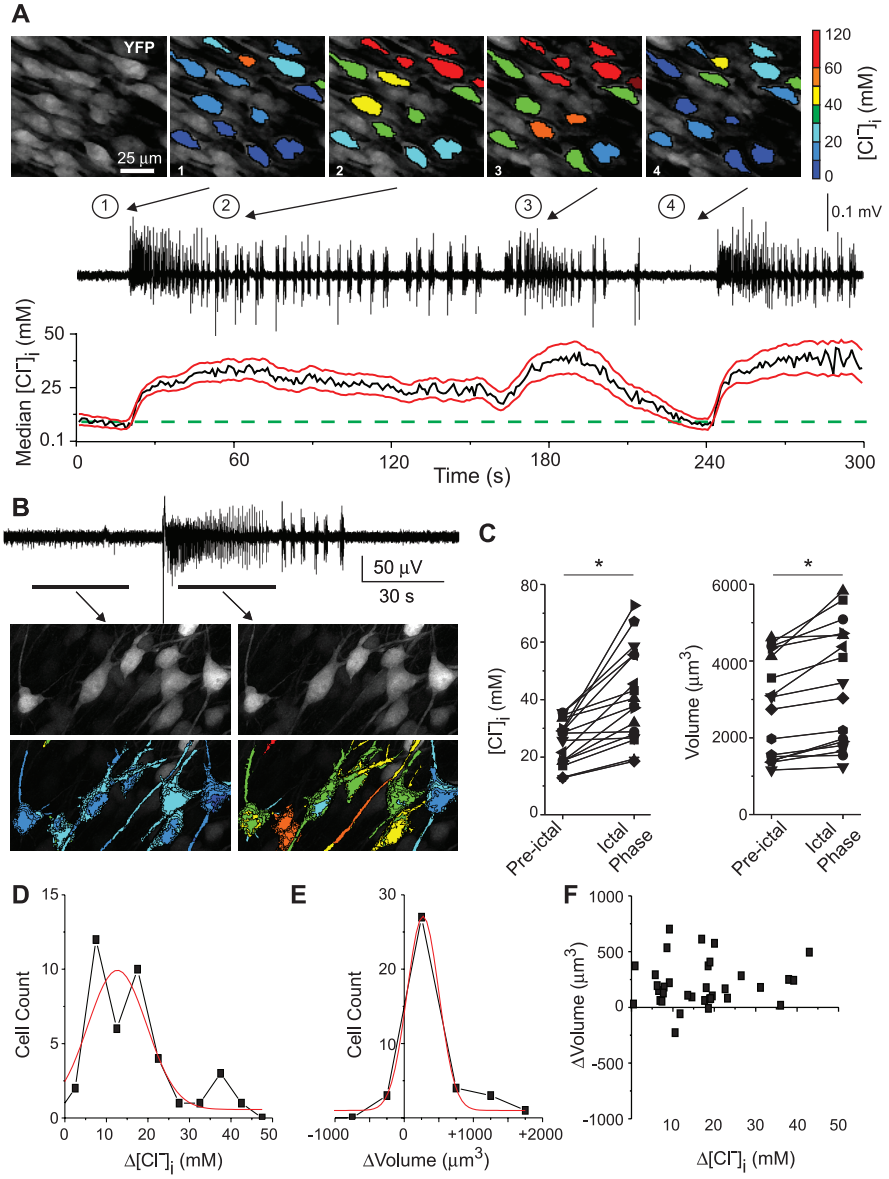

Fig. 4. $[Cl^-]_i$ and intracellular volume changes during ictal activity. (**A**) $[Cl^-]_i$ transients during spontaneous seizures in the CA1 pyramidal cell layer, organotypic hippocampal slice (DIV12). (Top) Pseudo-colored, two-photon images of CA1 neurons before and during seizures. (Middle) Extracellular field-potential recording. (Bottom) $[Cl^-]_i$ changes in a population of neurons (median, black; SD, red lines; green dotted line indicates initial $[Cl^-]_i$). (**B**) Extracellular recording of spontaneous seizure in CA1 region of organotypic hippocampal slice (DIV12). (Bottom) Two-photon microscopy z-stack image of neurons before and during spontaneous seizure. (**C**) $[Cl^-]_i$ and somatic volume changes in individual neurons during spontaneous seizure activity (*$P < 0.05$). (**D** to **F**) $[Cl^-]_i$ and somatic volume changes during recurrent seizures (n = 40 neurons; four slices).

of $[A]_o$ and $[A]_i$ on local $[Cl^-]_i$, and $[Cl^-]_o$ open possibilities for developmental and experience-dependent plasticity of E_{GABA} and $E_{glycine}$ at individual synapses, so that the variance in extracellular sulfated proteoglycans composes a potential locus of analog information storage and pathologically, a rich variety of antigens. (v) Pathological conditions that alter $[A]_o$ or $[A]_i$ will have secondary effects on both cell volume and $[Cl^-]_i$. This may explain the correlation between magnetic resonance imaging evidence of cytotoxic edema after brain injury and anticonvulsant-resistant seizures, which can occur when increased $[Cl^-]_i$ compromises $GABA_AR$-mediated inhibition (*15*, *40*). Thus, the magnitude and direction of $GABA_AR$ currents at individual synapses are among the wide variety of signaling functions subserved by intra- and extracellular macromolecular networks.

References and Notes

1. U. Misgeld, R. A. Deisz, H. U. Dodt, H. D. Lux, *Science* **232**, 1413–1415 (1986).
2. N. L. Chamberlin, R. Dingledine, *Brain Res.* **445**, 12–18 (1988).
3. F. J. Alvarez-Leefmans, E. Delpire, Eds., *Physiology and Pathology of Chloride Transporters and Channels in the Nervous System: From Molecules to Diseases* (Academic Press, San Diego, CA, 2009).
4. R. A. DeFazio, S. Keros, M. W. Quick, J. J. Hablitz, *J. Neurosci.* **20**, 8069–8076 (2000).
5. J. A. Payne, *Am. J. Physiol.* **273**, C1516–C1525 (1997).
6. T. Zeuthen, *J. Membr. Biol.* **234**, 57–73 (2010).
7. E. K. Hoffmann, I. H. Lambert, S. F. Pedersen, *Physiol. Rev.* **89**, 193–277 (2009).
8. R. D. Andrew, M. W. Labron, S. E. Boehnke, L. Carnduff, S. A. Kirov, *Cereb. Cortex* **17**, 787–802 (2007).
9. V. Balakrishnan *et al.*, *J. Neurosci.* **23**, 4134–4145 (2003).
10. J. Glykys *et al.*, *Neuron* **63**, 657–672 (2009).
11. S. Ebihara, K. Shirato, N. Harata, N. Akaike, *J. Physiol.* **484**, 77–86 (1995).
12. J. Yamada *et al.*, *J. Physiol.* **557**, 829–841 (2004).
13. R. Tyzio *et al.*, *Eur. J. Neurosci.* **27**, 2515–2528 (2008).
14. M. Martina, S. Royer, D. Paré, *J. Neurophysiol.* **86**, 2887–2895 (2001).
15. V. I. Dzhala *et al.*, *J. Neurosci.* **30**, 11745–11761 (2010).
16. J. Szabadics *et al.*, *Science* **311**, 233–235 (2006).
17. N. Doyon *et al.*, *PLOS Comput. Biol.* **7**, e1002149 (2011).
18. T. Kuner, G. J. Augustine, *Neuron* **27**, 447–459 (2000).
19. E. Gianazza, P. G. Righetti, *J. Chromatogr. A* **193**, 1–8 (1980).
20. A. Leaf, *Biochem. J.* **62**, 241–248 (1956).
21. F. J. Alvarez-Leefmans, S. M. Gamiño, L. Reuss, *J. Physiol.* **458**, 603–619 (1992).
22. C. E. Bandtlow, D. R. Zimmermann, *Physiol. Rev.* **80**, 1267–1290 (2000).
23. D. Isaev *et al.*, *J. Neurosci.* **27**, 11587–11594 (2007).
24. M. D. Plotkin, E. Y. Snyder, S. C. Hebert, E. Delpire, *J. Neurobiol.* **33**, 781–795 (1997).
25. E. Delpire *et al.*, *Proc. Natl. Acad. Sci. U.S.A.* **106**, 5383–5388 (2009).
26. A. P. Minton, *J. Biol. Chem.* **276**, 10577–10580 (2001).
27. R. J. Ellis, *Curr. Opin. Struct. Biol.* **11**, 114–119 (2001).
28. R. C. Poole, A. P. Halestrap, *Am. J. Physiol.* **264**, C761–C782 (1993).
29. E. Ruusuvuori, I. Kirilkin, N. Pandya, K. Kaila, *J. Neurosci.* **30**, 15638–15642 (2010).
30. N. O. Chahine, F. H. Chen, C. T. Hung, G. A. Ateshian, *Biophys. J.* **89**, 1543–1550 (2005).
31. T. Murakami, A. Ohtsuka, D. X. Piao, *Arch. Histol. Cytol.* **59**, 233–237 (1996).
32. B. B. Pond *et al.*, *J. Neurosci.* **26**, 1396–1406 (2006).
33. A. N. van den Pol, K. Obrietan, G. Chen, *J. Neurosci.* **16**, 4283–4292 (1996).
34. Y. Berdichevsky, V. Dzhala, M. Mail, K. J. Staley, *Neurobiol. Dis.* **45**, 774–785 (2012).
35. D. B. McClatchy, L. Liao, S. K. Park, J. D. Venable, J. R. Yates, *Genome Res.* **17**, 1378–1388 (2007).
36. J. Tanaka *et al.*, *Science* **319**, 1683–1687 (2008).
37. R. Frischknecht *et al.*, *Nat. Neurosci.* **12**, 897–904 (2009).
38. H. Song, M. Sokolov, *J. Proteome Res.* **8**, 346–351 (2009).
39. J. Ricka, T. Tanaka, *Macromolecules* **17**, 2916–2921 (1984).
40. H. C. Glass *et al.*, *J. Pediatr.* **159**, 731–735, e1 (2011).

Acknowledgments: This work was supported by National Institute of Neurological Disorders and Stroke, NIH, grant NS 40109-06 the Kennedy Endowment for Child Neurology and Mental Retardation. J.G. was supported by the American Epilepsy Society postdoctoral fellowship and NIH R25. K.E. was supported by The Japan Foundation for Pediatric Research. K.T.K. was supported by the Manton Center for Orphan Disease Research and NIH R25.

Supplementary Materials

www.sciencemag.org/content/343/6171/670/suppl/DC1
Materials and Methods
Figs. S1 to S10
Tables S1 and S2
References

2 September 2013; accepted 12 December 2013
10.1126/science.1245423

Oxytocin-Mediated GABA Inhibition During Delivery Attenuates Autism Pathogenesis in Rodent Offspring

Roman Tyzio,[1,2]* Romain Nardou,[3]* Diana C. Ferrari,[3]* Timur Tsintsadze,[1,2,3] Amene Shahrokhi,[3]† Sanaz Eftekhari,[3]† Ilgam Khalilov,[1,2] Vera Tsintsadze,[1,2] Corinne Brouchoud,[1,2] Genevieve Chazal,[1,2] Eric Lemonnier,[4] Natalia Lozovaya,[1,2] Nail Burnashev,[1,2] Yehezkel Ben-Ari[1,2,3]‡

We report that the oxytocin-mediated neuroprotective γ-aminobutyric acid (GABA) excitatory-inhibitory shift during delivery is abolished in the valproate and fragile X rodent models of autism. During delivery and subsequently, hippocampal neurons in these models have elevated intracellular chloride levels, increased excitatory GABA, enhanced glutamatergic activity, and elevated gamma oscillations. Maternal pretreatment with bumetanide restored in offspring control electrophysiological and behavioral phenotypes. Conversely, blocking oxytocin signaling in naïve mothers produced offspring having electrophysiological and behavioral autistic-like features. Our results suggest a chronic deficient chloride regulation in these rodent models of autism and stress the importance of oxytocin-mediated GABAergic inhibition during the delivery process. Our data validate the amelioration observed with bumetanide and oxytocin and point to common pathways in a drug-induced and a genetic rodent model of autism.

Autism is a developmental disorder characterized by restricted interest and communication impairment generated by genetic and environmental factors. Alterations of oxytocin signals that trigger labor and are instrumental for communication, notably, parental-infant interactions, are important in autism (*1*). Here, we characterized the cellular and network alterations that occur during the transition from fetal to postnatal life and subsequently in two animal models of autism: rats exposed in utero to valproate (VPA rats) and mice carrying the fragile X mutation (FRX mice). We focused on GABAergic inhibition, as this is deficient in human and animal models of autism, which leads to an imbalance between excitation and inhibition (*2*–*4*). In addition, during development, GABAergic currents shift from excitatory to inhibitory (*5*) because of a reduction of intracellular chloride concentration ($[Cl^-]_i$) mediated by a sequential expression of the main chloride importer (Na^+-K^+-$2Cl^-$ cotransporter, NKCC1) and the main chloride exporter KCC2 (*6*). Delivery in rodents is fundamental in this sequence, with an abrupt oxytocin-mediated reduction of $[Cl^-]_i$ levels that exerts neuroprotective (*7*) and analgesic (*8*) actions on newborns. We report that this sequence is abolished in hippocampal CA3 pyramidal neurons of VPA rats and FRX mice, and its restoration by administering bumetanide to the mother rescues the GABA developmental sequence and the autistic phenotype in rodent offspring.

In naïve rats (Fig. 1A and table S1) [see also (*7*)] and wild-type mice (Fig. 1D and table S1), the driving force of γ-aminobutyric acid type A ($GABA_A$) receptor $GABA_AR$ (DF_{GABA}) was elevated in fetal neurons on embryonic days 20 to 21 (E20 to E21) and reduced to adult values at postnatal days 15 to 30 (P15 to P30), with an abrupt reduction restricted to the delivery period (*9*). In contrast, DF_{GABA} remained elevated in

[1]Mediterranean Institute of Neurobiology (INMED), U901, INSERM, Marseille, France. [2]UMR 901, Aix-Marseille University, Marseille, France. [3]Neurochlore, Campus scientific de Luminy, 163 route de Luminy, Marseille 13273, Cedex 09, France. [4]Laboratoire de Neurosciences de Brest EA4685, Brest, France.

*These authors contributed equally to this work.
†On leave from Tehran University of Medical Sciences, Tehran, Iran.
‡Corresponding author. E-mail: yehezkel.ben-ari@inserm.fr

Science

Local Impermeant Anions Establish the Neuronal Chloride Concentration

J. Glykys, V. Dzhala, K. Egawa, T Balena, Y. Saponjian, K. V. Kuchibhotla, B. J. Bacskai, K. T. Kahle, T. Zeuthen, and K. J. Staley

Science, 343 (6171), • DOI: 10.1126/science.1245423

Causing Chloride Changes

Because intracellular chloride concentrations largely determine the direction and magnitude of current flow through $GABA_A$ channels, the stability of intracellular chloride concentration is important to maintain consistent synaptic inhibition. Glykys *et al.* (p. 670) examined the mechanisms by which chloride gradients in neurons are established, using chloride imaging with transgenically expressed clomeleon dye. Surprisingly, intracellular chloride was not primarily determined by transporters. Instead, subcellular gradients of immobile anions generated inverse chloride gradients.

Science (ISSN 1095-9203) is published by the American Association for the Advancement of Science. 1200 New York Avenue NW, Washington, DC 20005. The title *Science* is a registered trademark of AAAS.